EXTENDED PDF FORMAT
SPONSORED BY
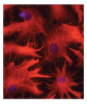
Travel Grants Available
Neuroscience 2014
Application Deadline: July 31st
>Apply Now
R&D systems
a bio-techne brand
www.rndsystems.com

De novo formation of a distinct coronary vascular population in neonatal heart

Xueying Tian *et al.*

Science **345**, 90 (2014);
DOI: 10.1126/science.1251487

This copy is for your personal, non-commercial use only.

If you wish to distribute this article to others, you can order high-quality copies for your colleagues, clients, or customers by clicking here.

Permission to republish or repurpose articles or portions of articles can be obtained by following the guidelines here.

The following resources related to this article are available online at www.sciencemag.org (this information is current as of July 3, 2014):

Updated information and services, including high-resolution figures, can be found in the online version of this article at:
http://www.sciencemag.org/content/345/6192/90.full.html

Supporting Online Material can be found at:
http://www.sciencemag.org/content/suppl/2014/07/02/345.6192.90.DC1.html

A list of selected additional articles on the Science Web sites **related to this article** can be found at:
http://www.sciencemag.org/content/345/6192/90.full.html#related

This article **cites 25 articles**, 8 of which can be accessed free:
http://www.sciencemag.org/content/345/6192/90.full.html#ref-list-1

This article has been **cited by** 1 articles hosted by HighWire Press; see:
http://www.sciencemag.org/content/345/6192/90.full.html#related-urls

This article appears in the following **subject collections:**
Development
http://www.sciencemag.org/cgi/collection/development

Downloaded from www.sciencemag.org on July 3, 2014

Science (print ISSN 0036-8075; online ISSN 1095-9203) is published weekly, except the last week in December, by the American Association for the Advancement of Science, 1200 New York Avenue NW, Washington, DC 20005. Copyright 2014 by the American Association for the Advancement of Science; all rights reserved. The title *Science* is a registered trademark of AAAS.

and ganglion cells at this stage had most likely switched off *Phox2b* or *Sox10*, respectively, because all nerve-associated cells equally expressed both genes a day earlier (and see below). The observed sequence of events suggests that the SOX10$^+$ cells, which then become SOX10$^+$/PHOX2b$^+$ double-positive, migrate along the nerve and reach in that way the site of ganglion formation, although a directed proliferation could also play a role. Accordingly, in *Neurog2* KO, where Jacobson's nerve is absent (Fig. 1), the stream of cells was absent (fig. S1). This scenario is not unique to the otic ganglion, because a similar sequence was evident for the sphenopalatine and cardiac ganglia (fig. S7).

Schwann cell precursors, which later give rise to myelinating and nonmyelinating Schwann cells, occupy embryonic nerves from E11 (*18*). We therefore explored whether the nerve-associated SOX10$^+$/PHOX2b$^+$ cells might be Schwann cell precursors. Like Schwann cell precursors and like otic ganglion cells (fig. S8), PHOX2b$^+$ Jacobson's nerve–associated cells were derived from the neural crest, as evidenced by Wnt1::Cre lineage tracing (Fig. 3). They expressed markers of neural crest (FOXD3, SOX2, and p75) and Schwann cell precursors (ErbB3, *Cadherin19*, and the myelin protein *PLP*) (Fig. 3). In contrast, none of them detectably expressed neuronal markers, such as NeuN and TUBB3, or the proneural factors *Neurog2* or *Ascl1* (fig. S9). *Ascl1* (but not *Neurog2*) was up-regulated in ganglion cells (fig. S9) in keeping with its later roles in parasympathetic ganglia (*19*). Thus, cranial nerve–associated parasympathetic precursors have all the hallmarks of Schwann cell precursors.

Because cranial nerve–associated cells have features of both autonomic and Schwann cell precursors, we tested whether they actually produced Schwann cells. In *Phox2b::Cre; ROSA^{tdTomato}* embryos (*13*), as early as E13.5, Jacobson's nerve was coated with SOX10$^+$/PHOX2b$^-$ cells that expressed tdTomato (Fig. 4A), confirming that PHOX2b$^+$ nerve-associated cells subsequently switch it off. At E16.5, several cranial nerves contained numerous tdTomato$^+$ cells intermingled with the fibers (Fig. 4B and fig. S10), most of them PHOX2b$^-$, an occasional one still expressing the gene (fig. S10). A different set of recombinase and reporter [*Phox2b::FLPo* (*20*) and *RC::Fela* (*21*)] (fig. S10) produced similar results. Many cranial nerve–associated PHOX2b$^-$ tdTomato$^+$ cells expressed the Schwann cell markers Oct6 at E16.5 and S100 at P7 (Fig. 4, C and D) (*18*), signs of their differentiation into Schwann cells. Thus, cranial Schwann cells derive in part from a contingent of nerve-associated cells with a history of *Phox2b* expression. Such cells, albeit sparser, were also associated with limb nerves (Fig. 4E and fig. S11), and, from E13.5 on, we found (in 9 out of 10 limbs) a small ganglion made of PHOX2b$^+$ neurons on the median nerve of the forelimb (Fig. 4, E and F), showing that the dual Schwann cell and neuron fate, although mostly associated with cranial nerves, is not unique to them. The persistence in the adult and physiological meaning, if any, of this new ganglion and the nature of its preganglionic innervation—known to control the survival of parasympathetic neurons (*22*)—remain to be determined.

Thus, parasympathetic ganglion neurons are derivatives of multifated Schwann cell precursors, known to give rise in vivo to melanocytes (*23*) and endoneurial fibroblasts (*24*) in addition to Schwann cells. The neuronal potential of these precursors, reported in vitro or after back transplantation for sciatic nerve–derived cells (*25*, *26*), is achieved during the normal development of cranial nerves. Accordingly, the numerous locations of parasympathetic ganglia throughout the head and trunk are specified by the pattern of cranial nerve outgrowths, a parsimonious way of hooking up pre- and postganglionic partners in development and, conceivably, of synchronizing their appearance in evolution.

REFERENCES AND NOTES

1. E. Kandel, J. Schwartz, T. Jessell, S. Siegelbaum, A. J. Hudspeth, *Principles of Neural Science, Fifth Edition* (McGraw Hill, New York, 2012).
2. W. W. Blessing, *The Lower Brainstem and Bodily Homeostasis* (Oxford Univ. Press, New York, 1997).
3. N. Le Douarin, C. Kalcheim, *The Neural Crest* (Cambridge Univ. Press, Cambridge, 1999).
4. Y. Takahashi, D. Sipp, H. Enomoto, *Science* **341**, 860–863 (2013).
5. E. Coppola *et al*., *Proc. Natl. Acad. Sci. U.S.A.* **107**, 2066–2071 (2010).
6. J. Ai *et al*., *Neuroscience* **149**, 845–860 (2007).
7. C. Fode *et al*., *Neuron* **20**, 483–494 (1998).
8. M. Florio *et al*., *Development* **139**, 2308–2320 (2012).
9. D. Brockschnieder, Y. Pechmann, E. Sonnenberg-Riethmacher, D. Riethmacher, *Genesis* **44**, 322–327 (2006).
10. S. Harbinder *et al*., *Proc. Natl. Acad. Sci. U.S.A.* **94**, 13128–13133 (1997).
11. R. Waldmann, G. Champigny, N. Voilley, I. Lauritzen, M. Lazdunski, *J. Biol. Chem.* **271**, 10433–10436 (1996).
12. A. Pattyn, X. Morin, H. Cremer, C. Goridis, J. F. Brunet, *Development* **124**, 4065–4075 (1997).
13. F. D'Autréaux, E. Coppola, M.-R. Hirsch, C. Birchmeier, J.-F. Brunet, *Proc. Natl. Acad. Sci. U.S.A.* **108**, 20018–20023 (2011).
14. Y. Echelard, G. Vassileva, A. P. McMahon, *Development* **120**, 2213–2224 (1994).
15. M. C. Tiveron, M. R. Hirsch, J. F. Brunet, *J. Neurosci.* **16**, 7649–7660 (1996).
16. M. Wegner, C. C. Stolt, *Trends Neurosci.* **28**, 583–588 (2005).
17. A. Pattyn, X. Morin, H. Cremer, C. Goridis, J. F. Brunet, *Nature* **399**, 366–370 (1999).
18. K. R. Jessen, R. Mirsky, *Nat. Rev. Neurosci.* **6**, 671–682 (2005).
19. M. R. Hirsch, M. C. Tiveron, F. Guillemot, J. F. Brunet, C. Goridis, *Development* **125**, 599–608 (1998).
20. M.-R. Hirsch, F. d'Autréaux, S. M. Dymecki, J.-F. Brunet, C. Goridis, *Genesis* **51**, 506–514 (2013).
21. P. Jensen *et al*., *Nat. Neurosci.* **11**, 417–419 (2008).
22. S. Furber, R. W. Oppenheim, D. Prevette, *J. Neurosci.* **7**, 1816–1832 (1987).
23. I. Adameyko *et al*., *Cell* **139**, 366–379 (2009).
24. N. M. Joseph *et al*., *Development* **131**, 5599–5612 (2004).
25. S. J. Morrison, P. M. White, C. Zock, D. J. Anderson, *Cell* **96**, 737–749 (1999).
26. P. M. White *et al*., *Neuron* **29**, 57–71 (2001).

ACKNOWLEDGMENTS

We thank M. Lazdunski for the *ASIC2a^{G430F}* clone; C. Birchmeier, T. Müller, and M. Wegner for antibodies; M.-C. Tiveron for the original discovery of the limb ganglion; V. Michel for preliminary experiments; the imaging facilities of IBENS and Institut de la Vision, B. Mathieu, and D. Godefroy for technical assistance; and C. Goridis for helpful discussions. This work was supported by the Agence Nationale de la Recherche (ANR-12-BSV4-0007-01) and Investissements d'Avenir (ANR-10-LABX-54 MEMO LIFE and ANR-11-IDEX-0001-02 PSL* Research University) (to J.-F.B.); Fédération pour la Recherche sur le Cerveau (to Institut de la Vision); and NIH grants R01 DK067826, R21 DA023643, and P01 HD036379 (to S.D.). G.G.C. was funded by the Fondazione CARIPLO, Milan, Italy, and I.-E.M. received a Ph.D. studentship.

SUPPLEMENTARY MATERIALS

www.sciencemag.org/content/345/6192/87/suppl/DC1
Materials and Methods
Figs. S1 to S11
References (*27*–*33*)

12 March 2014; accepted 27 May 2014
Published online 12 June 2014;
10.1126/science.1253286

VESSEL FORMATION

De novo formation of a distinct coronary vascular population in neonatal heart

Xueying Tian,[1*] Tianyuan Hu,[1*] Hui Zhang,[1*] Lingjuan He,[1*] Xiuzhen Huang,[1] Qiaozhen Liu,[1] Wei Yu,[1] Liang He,[1] Zhen Yang,[2] Yan Yan,[2] Xiao Yang,[3] Tao P. Zhong,[4] William T. Pu,[5,6] Bin Zhou[1]†

The postnatal coronary vessels have been viewed as developing through expansion of vessels formed during the fetal period. Using genetic lineage tracing, we found that a substantial portion of postnatal coronary vessels arise de novo in the neonatal mouse heart, rather than expanding from preexisting embryonic vasculature. Our data show that lineage conversion of neonatal endocardial cells during trabecular compaction generates a distinct compartment of the coronary circulation located within the inner half of the ventricular wall. This lineage conversion occurs within a brief period after birth and provides an efficient means of rapidly augmenting the coronary vasculature. This mechanism of postnatal coronary vascular growth provides avenues for understanding and stimulating cardiovascular regeneration following injury and disease.

Coronary artery disease causes myocardial infarction, the leading cause of death worldwide. How coronary arteries develop is a fundamental biological question with important ramifications for human health and disease (*1*). Defining the developmental programs that give rise to the coronary arteries will provide critical information for regenerative approaches to congenital and adult heart disease (*2*–*4*). Most previous studies of coronary developmental origins have focused on the midgestation stage, when coronary vessels initially form

over the heart (*5*–*11*). Postnatal coronary vessels were presumed to arise from these embryonic coronary vessels, but few studies have examined postnatal coronary artery growth, and this assumption has not been rigorously tested.

Embryonic coronary vessels initially form as a vascular plexus that covers the outer surface of the heart (*6*, *11*). The underlying heart muscle is composed of compact myocardium, the free walls of the ventricular chambers, and trabecular myocardium, the fingerlike projections into the chambers (*12*). Compact myocardium develops intramyocardial coronary vessels, whereas trabecular myocardium largely lacks intramyocardial vessels and exchanges nutrients with the surrounding blood within the ventricular chambers. During rapid postnatal ventricular growth, the trabecular myocardium undergoes "compaction" and coalesces with compact myocardium (*12*). This new layer of compact myocardium becomes richly supplied with coronary vessels. The developmental program for postnatal vascularization of this newly compacted myocardium was previously unknown.

Here, we used tamoxifen-inducible Cre recombinase controlled by the apelin promoter (Apln-CreER) to permanently label embryonic vascular endothelial cells (VECs) of coronary vessels (*11*). A single tamoxifen injection at mouse embryonic day 10.5 (E10.5) induced recombination of Cre reporter alleles, which indelibly labeled early coronary sprouts and their progeny (*11*). This treatment allowed us to almost completely label coronary vessels in the embryonic ventricle wall at E15.5 (Fig. 1). We designated this coronary vascular population (CVP) labeled by Apln-CreER activation at E10.5 as the first CVP. We followed the first CVP's fate in postnatal days 0 to 7 (P0 to P7) neonatal hearts and found that labeled coronary vessels were confined to the outer half of the myocardial wall at P3 and P7 (Fig. 1). In neonatal hearts, progressive myocardial compaction was accompanied by accumulation of unlabeled coronary vessels in the inner half of the myocardial wall at P3 and P7 (Fig. 1). These unlabeled platelet endothelial cell adhesion molecule–positive ($PECAM^+$) cells were bona fide coronary vessels because they were positive for the coronary VEC markers APLN (*6*) and fatty acid binding protein 4 (FABP4) (*13*) (fig. S1 to S3). These data demonstrate that the newly formed coronary vessels in the inner myocardial wall of neonatal heart are not derivatives of the first CVP, which indicates that they form de novo from an alternative source.

[1]Key Laboratory of Nutrition and Metabolism, Institute for Nutritional Sciences, Shanghai Institutes for Biological Sciences, Graduate School of the Chinese Academy of Sciences, Chinese Academy of Sciences, Shanghai, 200031, China. [2]Zhongshan Hospital, Fudan University, Shanghai 200032, China. [3]State Key Laboratory of Proteomics, Institute of Biotechnology, Beijing 100071, China. [4]State Key Laboratory of Genetic Engineering, School of Life Sciences, Fudan University, Shanghai 200433, China. [5]Harvard Stem Cell Institute, Harvard University, Cambridge, MA 02138, USA. [6]Department of Cardiology, Children's Hospital Boston, 300 Longwood Avenue, Boston, MA 02115, USA.
*These authors contributed equally to this work. **†Corresponding author. E-mail: zhoubin@sibs.ac.cn**

To get a holistic view of coronary vascular development of the entire heart, we fate-mapped coronary VECs by Apln-CreER labeling at different times during heart development. Coronary vessels emerged in three temporal waves (fig. S4). By E10.5, the first CVP had emerged in the first wave and had formed the coronary vessels of the fetal ventricular free wall (fig. S5, A and B) and postnatal outer myocardial wall (fig. S4C). However, very few VECs of the ventricular septum were labeled by E10.5 tamoxifen induction (figs. S4B and S5B). Tamoxifen administration at E13.5 identified a second wave of coronary vessel development that formed most of the robust vascular supply of the interventricular septum during septal myocardial compaction (figs. S4D and S5C) (*12*). Labeling of these cells by tamoxifen at E13.5, but not E10.5, therefore indicates de novo formation of these septal vessels from a source other than the first CVP. The third wave occurred in the neonatal period, and similarly to the second wave, its emergence also accompanied trabecular compaction (fig. S4G). This neonatal wave of de novo vessel formation occurred in the inner myocardial wall and remained spatially segregated from the coronary vessels formed by the first and second wave (fig. S4H).

We next sought to define the developmental origin for the de novo formed vessels that did not originate from the first CVP. We generated inducible Nfatc1-CreER;$Rosa26^{RFP/+}$ mice (fig. S6, A and B), in which Nfatc1 regulatory elements direct selective expression of CreER to the endocardium (*14*). Staining of estrogen receptor (ESR) showed expression of CreER in atrial and ventricular endocardial cells in early developing heart (Fig. 2A and fig. S6, C and D). We administered tamoxifen at E8.0 to E8.5 to label E8.5 to E9.5 endocardial cells before the formation of coronary vessels (Fig. 2B) and analyzed embryos at multiple subsequent time points. Sinus venosus endocardium did not express CreER and was not labeled (see SV in Fig. 2A and fig. S7A). Nfatc1-CreER specifically labeled endocardial cells but not coronary VECs in the myocardial free wall (fig. S7, B and C). This result of inducible genetic labeling driven by Nfatc1-CreER differed from that of a previous report using constitutively active Nfatc1-Cre (see supplementary text). At P0, Nfatc1-CreER labeled 72.2% of neonatal ventricular endocardial cells and did not significantly label free wall VECs (fig. S7, D and E). In P7 hearts, 76.7 ± 5.4% of VECs in the inner myocardial wall expressed the red fluorescent protein (RFP) lineage tracer (Fig. 2C). A subset of nonlabeled VECs in the inner myocardial wall may arise from embryonic vessels or epicardium. In contrast to the inner myocardial wall, fewer VECs of the outer myocardial wall were labeled by Nfatc1-CreER (Fig. 2C). Together, these data indicate that inner myocardial wall VECs arise by lineage conversion of neonatal endocardial cells during trabecular compaction.

We also investigated the contribution of endocardial cells labeled by Nfatc1-CreER (pulse activated by tamoxifen at E8.0 to E8.5) to VECs of the interventricular septum. In both embryonic and neonatal hearts, Nfatc1-CreER labeled the majority of coronary VECs within the interventricular septum (fig. S6E). These data indicate that the interventricular septum, like the inner myocardial wall, is vascularized by lineage conversion of endocardial cells to coronary VECs.

The inverse and nearly exclusive relation between the Apln-CreER and Nfatc1-CreER fate maps was striking (fig. S8A). This result indicates that the postnatal coronary vasculature originates from two distinct CVPs that arise through different developmental mechanisms and remain spatially segregated in their location. The first CVP, labeled by Apln-CreER induced with tamoxifen at E10.5, derives from sub-epicardial precursors that generate the initial coronary vascular plexus of the fetal hearts (*6*, *11*) and ultimately gives rise to the VECs of the outer myocardial wall of the neonatal hearts (Fig. 1). Nfatc1-CreER labels ventricular endocardial cells, which give rise to a second CVP that ultimately irrigates the interventricular septum and VECs of the inner myocardial wall of the neonatal hearts (fig. S6E and Fig. 2C).

We next measured the relative vascular territory occupied by first and second CVPs in adult heart ventricle. Because labeling efficiency was higher when we used Apln-CreER rather than Nfatc1-CreER, we quantified with Apln-CreER labeling the relative myocardial volume irrigated by first CVP (RFP-labeled) and second CVP (unlabeled) (fig. S8, B and C). We examined serial sections spanning the entire heart at P0, P3, P7, P28, and P63 (Fig. 3A and figs. S8 and S9). At P0, the first CVP existed in 42% of the ventricular myocardium, whereas the second CVP was confined to the ventricular septum and supplied 24% of the ventricle myocardium (Fig. 3B). Trabeculae, lacking intramyocardial vessels, were still present along the luminal surface of the ventricles and accounted for the remaining 34% of the ventricular myocardium (Fig. 3B). By P7, trabecular myocardium transformed into compact myocardium, which was populated by the second CVP (Fig. 3B). In the P28 and P63 adult heart, a strong boundary was maintained at the interface of the first and second CVPs throughout the entire heart (Fig. 3A and figs. S9 and S8E). These data indicate that the vascular territory supplied by these developmentally distinct CVPs remains spatially segregated in the adult heart and that expansion of the second CVP accounts disproportionately for postnatal coronary vascular expansion (fig. S10).

To begin to understand how neonatal endocardial cells transform from a single sheet lining the heart lumen into many tube-shaped blood vessels, we observed their association with the basement membrane of trabecular myocardium during myocardial compaction. COL3A1, an extracellular matrix protein, is part of the trabecular basement membrane located just beneath the endocardial layer at P0. During subsequent myocardial compaction, COL3A1 was not degraded and left a historical mark of the remodeled trabecular protrusions (fig. S11A). Endocardial cells in the trabecular protrusions resided on the

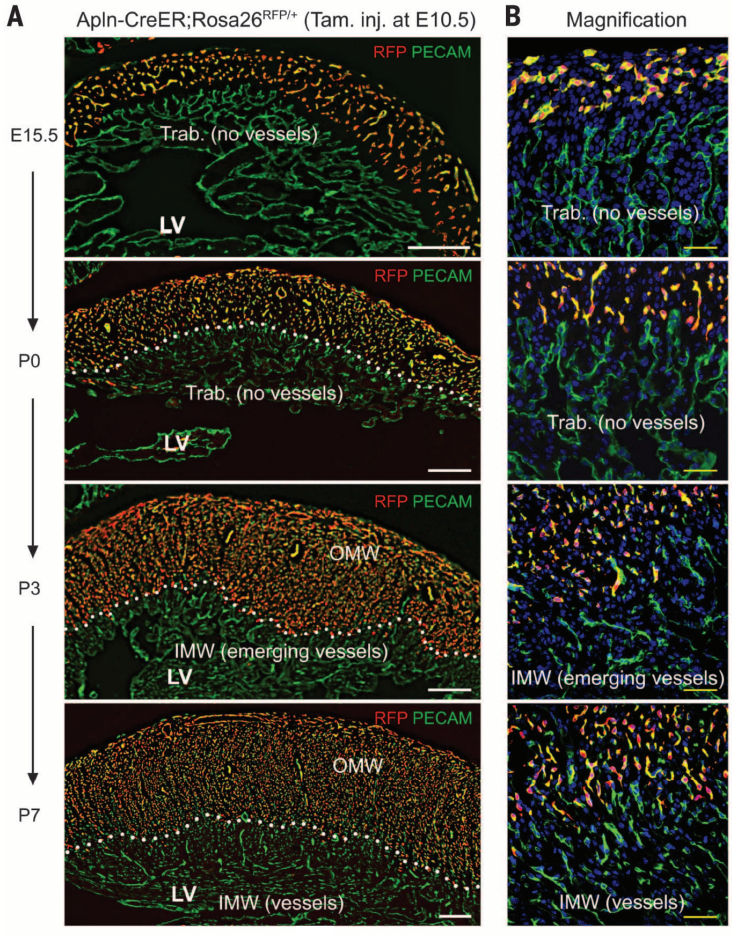

Fig. 1. Derivatives of embryonic coronary vessels do not expand into the inner myocardial wall of the neonatal heart. (**A** and **B**) Embryonic coronary vessels were RFP-labeled by tamoxifen treatment of Apln-CreER;Rosa26$^{RFP/+}$ embryos at E10.5. In the neonatal heart, these VECs, derived from embryonic coronary vessels, occupied the outer portion of the compact myocardium, defined as the outer myocardial wall (OMW). The remaining, RFP-negative portion of the compact myocardium was defined as the inner myocardial wall (IMW). White dotted lines highlight the inner border of left ventricular myocardium occupied by embryonically labeled vessels. From P0 to P7, trabecular myocardium (Trab.) transformed into compact myocardium where new coronary vessels arise. White scale bar, 200 μm; yellow scale bar, 50 μm. LV, left ventricle.

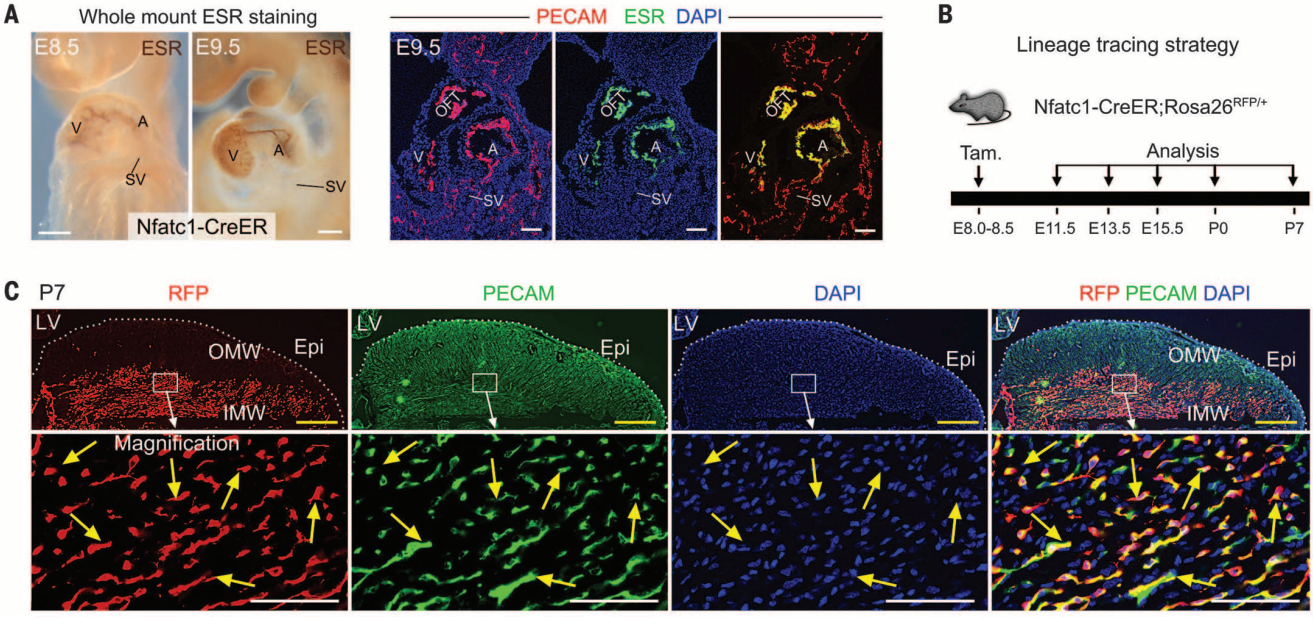

Fig. 2. Neonatal endocardial cells contribute to the de novo formed coronary vessels in the inner myocardial wall. (**A**) CreER was expressed in atrial and ventricular endocardium, but not sinus venosus, at E8.5 and E9.5. CreER was visualized by staining for the estrogen receptor (ESR) portion of the CreER fusion protein. V, ventricle; A, atrium; OFT, outflow tract; SV, sinus venosus. (**B**) Lineage tracing strategy using Nfatc1-CreER;Rosa26$^{RFP/+}$ line. Tamoxifen was injected at E8.0 to E8.5, and hearts were collected at later stages. (**C**) Immunostaining of genetic marker RFP and endothelial cell marker PECAM on P7 heart sections. Nfatc1-CreER–labeled endocardial cells contribute to the majority of VECs (76.7 ± 5.4%, yellow arrows) in the IMW, but not VECs in the OMW. White scale bar, 100 μm, yellow scale bar, 500 μm. n = 3 to 5 embryos examined at each time point.

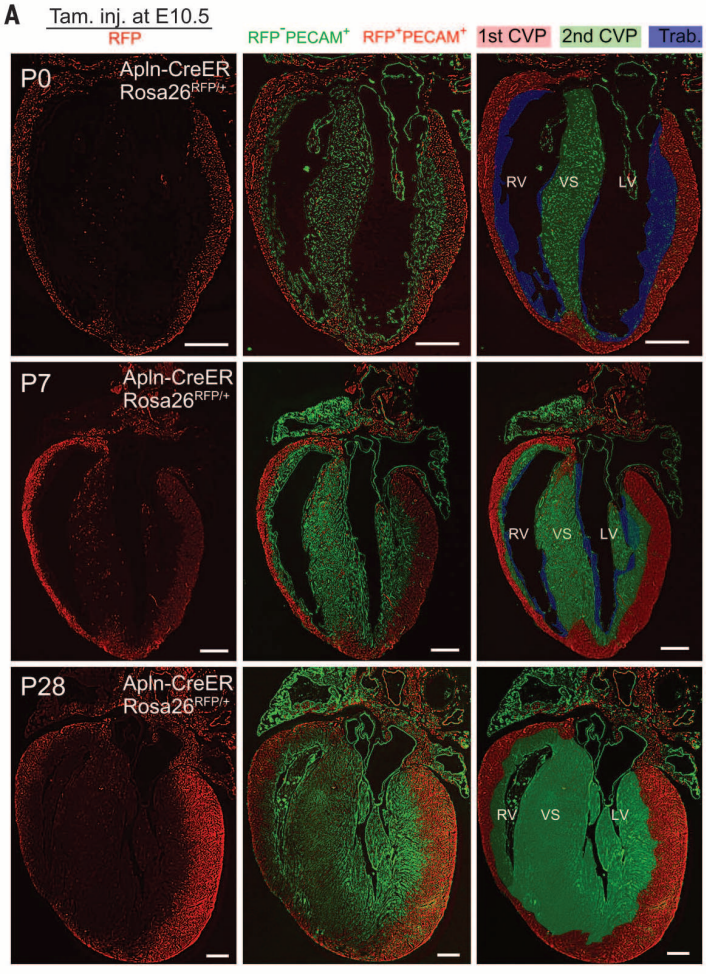

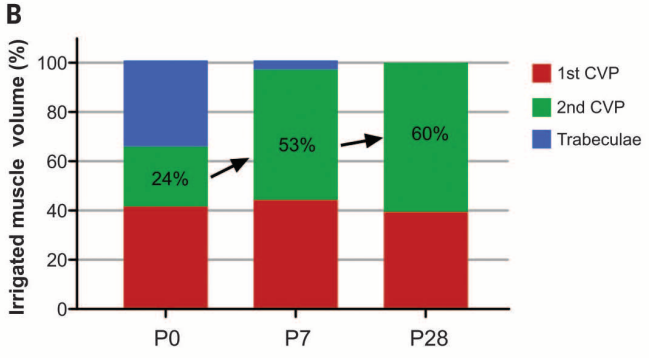

Fig. 3. First and second CVPs irrigate mutually exclusive regions of the myocardium of the adult heart. (**A**) Long-axis sections of mouse heart delineating the temporal evolution of first CVP (red), second CVP (green), and trabecular regions (blue) during the neonatal-to–adult heart transition. The first CVP was defined as the vessels genetically labeled (PECAM$^+$;RFP$^+$, pseudo-color red) by tamoxifen treatment of Apln-CreER;Rosa26$^{RFP/+}$ embryos at E10.5. The second CVP was defined as the remaining unlabeled intramyocardial vessels (PECAM$^+$;RFP$^-$, pseudo-color green). Trabecular myocardium was identified as the myocardium lacking intramyocardial vessels (PECAM$^-$;RFP$^-$). Shading in the right column indicates regions annotated as occupied by first CVP, second CVP or trabecular myocardium based on staining patterns. Images are representative of three to six hearts for each time point. White scale bar, 0.5 mm. (**B**) Relative ventricular myocardial volume occupied by first CVP, second CVP, or trabecular myocardium during postnatal heart growth. Note the rapid expansion of the myocardium irrigated by second CVP and diminution of the trabecular myocardium between P0 and P7. n = 3 to 6 for each time point.

Fig. 4. Neonatal endocardial cells were trapped in the inner myocardial wall. (**A**) Coronary vessels forming in the myocardial wall were labeled by tamoxifen treatment of Apln-CreER;Rosa26$^{mTmG/+}$ mice at P1.5 and analyzed at P3. Region (**B**) represents the luminal surface and contains unremodeled trabecular myocardium that persists at this stage. Yellow arrowheads indicate PECAM$^+$ endothelial cells that are not labeled by Apln-CreER and that reside on the basement membrane, indicative of endocardial cells. Region (**C**) represents the inner myocardial wall, containing PECAM$^+$ endothelial cells that are labeled by Apln-CreER and that reside within myocardium rather than on COL3A1 basement membrane, identifying them as tubelike coronary VECs (white arrowheads). White scale bar, 100 μm, yellow scale bar, 10 μm.

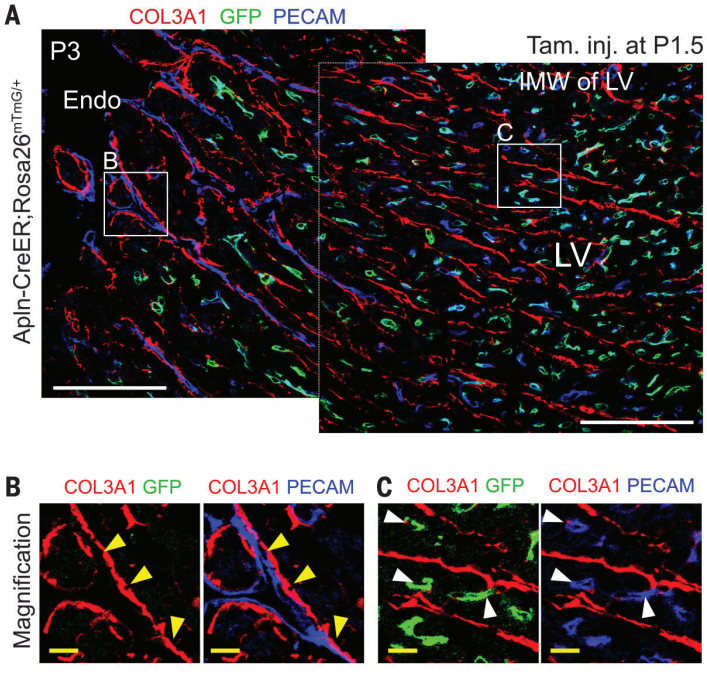

basement membrane at P0 (fig. S11, B and C). However, at P7, endocardial cells and their derivatives (labeled by Tie2-Cre or VE Cad-CreER) were no longer aligned with COL3A1 strands but rather took up intramyocardial positions (P7 in fig. S11, B and C). To better visualize the process by which P0 endocardium transforms into intramyocardial VECs at P7, we studied an intermediary stage (P3) when hearts contain both unremodeled trabeculae (Fig. 4B) and actively compacting regions (Fig. 4C). We labeled developmental intermediates by treating Apln-CreER; $Rosa26^{mTmG/+}$ mice with tamoxifen at P1.5 (Fig. 4A). Trapped endothelial cells remote from the basement membrane adopted the morphology of individual capillary-like cells and were marked by the VEC genetic lineage tracer (green fluorescent protein, see GFP in Fig. 4C), whereas endothelial cells facing the ventricular lumen and residing on the basement membrane retained sheetlike morphology and did not express VEC lineage tracer, consistent with endocardial identity (Fig. 4B). These observations suggest that myocardial compaction traps sheets of endocardial cells, which convert to the VEC lineage and translocate to an intramyocardial location.

We investigated conditions that might promote endocardium to VEC transition in the neonatal heart. Hypoxyprobe, a hypoxia-sensitive chemical probe, indicated that rapid expansion of the compact myocardium by trabecular coalescence in the first several postnatal days of life creates a hypoxic environment within the inner myocardial wall (fig. S12). Expression of hypoxia inducible factor 1α (*Hif1α*) and vascular endothelial growth factor A *Vegfa*, genes known to be up-regulated by hypoxia, increased in the inner myocardial wall of the P1 and P3 neonatal hearts (fig. S12, B and C). This corresponds to the region in which we observed endocardial to VEC lineage conversion, suggesting that hypoxia and its resulting up-regulation of the key angiogenic factor Vegfa contribute to this process.

Our work reveals a mechanism by which trabecular coalescence and endocardial-to-VEC lineage conversion drive vascular expansion in the postnatal heart. Why does coronary vascular growth in this setting rely on this alternative mechanism, rather than occurring through more typical angiogenic sprouting from preexisting vessels? The transition from fetal to postnatal circulation acutely increases the hemodynamic burden on the left ventricle. To accommodate this increased workload, we reason that mammals developed trabecular myocardium as a reservoir of new cardiomyocytes that is quickly recruited after birth through myocardial compaction to increase neonatal left ventricular mass. In addition to cardiomyocytes, this myocardial reservoir also contains coronary vessel precursors in the form of endocardial cells. Trabeculae coalesce during neonatal myocardial compaction causes regional hypoxia that stimulates the trapped neonatal endocardial cells to form the vascular supply for the newly compacted myocardium. This mechanism likely allows more rapid vascular and myocardial growth than angiogenic sprouting of the first CVP from the periphery. Understanding this endogenous mechanism for rapidly developing a functional vascular supply has important implications for cardiac diseases and cardiac regenerative medicine (*4*).

REFERENCES AND NOTES

1. P. R. Riley, N. Smart, *Cardiovasc. Res.* **91**, 260–268 (2011).
2. B. A. Yi, O. Wernet, K. R. Chien, *J. Clin. Invest.* **120**, 20–28 (2010).
3. N. Smart *et al.*, *Nature* **445**, 177–182 (2007).
4. E. R. Porrello *et al.*, *Science* **331**, 1078–1080 (2011).
5. H. S. Bennett, *Am. J. Anat.* **60**, 27–53 (1936).
6. K. Red-Horse, H. Ueno, I. L. Weissman, M. A. Krasnow, *Nature* **464**, 549–553 (2010).
7. T. C. Katz *et al.*, *Dev. Cell* **22**, 639–650 (2012).
8. B. Wu *et al.*, *Cell* **151**, 1083–1096 (2012).
9. P. Riley, *Nature* **464**, 498–499 (2010).
10. G. del Monte, P. Richard, *Cell* **151**, 932 (2012).
11. X. Tian *et al.*, *Cell Res.* **23**, 1075–1090 (2013).
12. D. Sedmera, T. Pexieder, M. Vuillemin, R. P. Thompson, R. H. Anderson, *Anat. Rec.* **258**, 319–337 (2000).
13. H. Elmasri *et al.*, *FASEB J.* **23**, 3865–3873 (2009).
14. B. Zhou *et al.*, *Development* **132**, 1137–1146 (2005).

ACKNOWLEDGMENTS

We thank K. Red-Horse, Y. Chen, and N. Jin for insightful discussions and R. Adams, H. Zeng, Z. Yang, T. Quertermous, J. Rossant, and A. Nagy for mouse strains. This work was supported by National Basic Research Program of China (2012CB945102 and 2013CB945302), National Natural Science Foundation of China (91339104, 31271552, 31222038, 31301188), Chinese Academy of Sciences (Hundred Talents Program and KSCX2-EW-R-09), Shanghai Pujiang Program (11PJ1411400) and Basic Research Key Project (14JC1407400), Organization Department of the CPC Central Committee Bajian Talents Program, AstraZeneca, Sanofi-Aventis Shanghai Institutes for Biological Sciences (SA-SIBS) Fellowship, Postdoc Fund (SIBS-2013KIP311, China-2013M541561), NIH (2 R01 HL094683), and American Heart Association Established Investigator Award to W.T.P.

SUPPLEMENTARY MATERIALS

www.sciencemag.org/content/345/6192/90/suppl/DC1
Materials and Methods
Figs. S1 to S12
References (*15*–*25*)

29 January 2014; accepted 22 May 2014
10.1126/science.1251487

PLANT-FUNGAL ECOLOGY

Niche engineering demonstrates a latent capacity for fungal-algal mutualism

Erik F. Y. Hom[1,2]*† and Andrew W. Murray[1,2]*

Mutualistic symbioses shape the evolution of species and ecosystems and catalyze the emergence of biological complexity, yet how such symbioses first form is unclear. We show that an obligate mutualism between the yeast *Saccharomyces cerevisiae* and the alga *Chlamydomonas reinhardtii*—two model eukaryotes with very different life histories—can arise spontaneously in an environment requiring reciprocal carbon and nitrogen exchange. This capacity for mutualism is phylogenetically broad, extending to other *Chlamydomonas* and fungal species. Furthermore, we witnessed the spontaneous association of *Chlamydomonas* algal cells physically interacting with filamentous fungi. These observations demonstrate that under specific conditions, environmental change induces free-living species to become obligate mutualists and establishes a set of experimentally tractable, phylogenetically related, synthetic systems for studying the evolution of symbiosis.

Mutualistic symbioses—beneficial associations between different species involving persistent physical contact and physiological coupling—are central to many evolutionary and ecological innovations (*1*–*3*). These include the origin of eukaryotic cells, the colonization of land by plants, coral reefs, and the gut microbiota of insects and animals (*4*, *5*). Despite their ubiquity and importance, we understand little about how mutualistic symbioses form between previously free-living organisms (*5*, *6*). Like speciation, the birth of novel symbioses has rarely been witnessed, making it difficult to determine if coevolution occurs before symbiosis begins or if chance ecological encounters initiate new symbioses (*5*, *7*). Such "ecological fitting" (*8*, *9*) occurs when both a particular environment and previously evolved traits allow a set of species to complement each other, giving rise to novel interactions without the need for prior coevolutionary adaptation.

We tested two genetically tractable organisms, the budding yeast *Saccharomyces cerevisiae* and the green alga *Chlamydomonas reinhardtii*, to determine if a reciprocal exchange of carbon and nitrogen would lead to obligate mutualism between algae and fungi such as those that occur naturally (*10*–*13*). In our scheme (Fig. 1A), *S. cerevisiae* metabolizes glucose to carbon dioxide (CO_2), a carbon source that *C. reinhardtii* fixes via photosynthesis, and *C. reinhardtii* reduces nitrite (NO_2^-) into ammonia (NH_3) (*14*), which yeast can use as a nitrogen source. Coculturing

[1]Department of Molecular and Cellular Biology, Harvard University, Cambridge, MA 02138, USA. [2]Faculty of Arts and Sciences Center for Systems Biology, Harvard University, Cambridge, MA 02138, USA.
***Corresponding author. E-mail: erik@fyhom.com; amurray@mcb.harvard.edu** †Present address: Department of Biology, University of Mississippi, University, MS 38677, USA.